Journal of proteome research

Article

Cite This: J. Proteome Res. XXXX, XXX, XXX−XXX

pubs.acs.org/jpr

Integrated Dissection of Cysteine Oxidative Post-translational Modification Proteome During Cardiac Hypertrophy

Jie Wang,[†,⊥,¶] Howard Choi,[†,§,⊥,¶] Neo C. Chung,[⊥] Quan Cao,[†,⊥] Dominic C. M. Ng,[†,⊥] Bilal Mirza,[†,⊥] Sarah B. Scruggs,[†,⊥] Ding Wang,[†,⊥] Anders O. Garlid,[†,⊥] and Peipei Ping*[,†,‡,§,⊥]

[†]Departments of Physiology, [‡]Medicine (Cardiology), [§]Bioinformatics, and [⊥]NIH BD2K Center of Excellence for Biomedical Computing, University of California Los Angeles, Los Angeles, California 90095, United States

Supporting Information

ABSTRACT: Cysteine oxidative modification of cellular proteins is crucial for many aspects of cardiac hypertrophy development. However, integrated dissection of multiple types of cysteine oxidative post-translational modifications (O-PTM) of proteomes in cardiac hypertrophy is currently missing. Here we developed a novel discovery platform that encompasses a customized biotin switch-based quantitative proteomics pipeline and an advanced analytic workflow to comprehensively profile the landscape of cysteine O-PTM in an ISO-induced cardiac hypertrophy mouse model. Specifically, we identified a total of 1655 proteins containing 3324 oxidized cysteine sites by at least one of the following three modifications: reversible cysteine O-PTM, cysteine sulfinylation ($CysSO_2H$), and cysteine sulfonylation ($CysSO_3H$). Analyzing the hypertrophy signatures that are reproducibly discovered from this computational workflow unveiled four biological processes with increased cysteine O-PTM. Among them, protein phosphorylation, creatine metabolism, and response to elevated Ca^{2+} pathways exhibited an elevation of cysteine O-PTM in early stages, whereas glucose metabolism enzymes were increasingly modified in later stages, illustrating a temporal regulatory map in cardiac hypertrophy. Our cysteine O-PTM platform depicts a dynamic and integrated landscape of the cysteine oxidative proteome, through the extracted molecular signatures, and provides critical mechanistic insights in cardiac hypertrophy. Data are available via ProteomeXchange with identifier PXD010336.

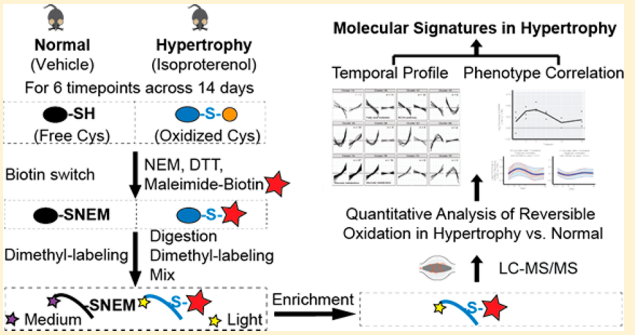

KEYWORDS: *cysteine oxidative modification, cardiac hypertrophy, redox proteomics, computational workflow, cubic spline, biotin switch*

INTRODUCTION

Cardiac hypertrophy is an adaptive response of the heart to pressure overload and a risk factor for heart failure and sudden cardiac death.[1−3] The complex and dynamic pathophysiological mechanisms surrounding cardiac hypertrophy have been the focus of many investigations seeking therapeutic strategies. Reactive oxygen and nitrogen species (RO/NS) have been recognized as second messengers that mediate important biological processes during the development of cardiac hypertrophy.[2,4] As a major target of RO/NS, protein cysteine residues can act as molecular switches and undergo various types of oxidative post-translational modifications (O-PTM),[5] which can alter protein 3D structure and activity in cellular signaling, adaptive and maladaptive cardiac responses.[4,6,7] Major cysteine O-PTM types observed in cardiac muscle include reversible (S-nitrosylation, S-glutathionylation, sulfenic acid, inter- and intramolecular disulfide bonds, and S-sulfhydration) and irreversible sulfinic acid ($CysSO_2H$) or sulfonic acid ($CysSO_3H$) modifications.[4,8,9] As dysregulation of cysteine O-PTM is directly associated with disease pathology,[4,10] identification and characterization of cysteine O-PTM could yield a wider range of biomarkers and therapeutic targets for diseases characterized by oxidative stress. Because of the complexity of the cysteine oxidative proteome, elucidation of these molecular signatures during hypertrophy progression is currently lacking. Biotin switch assays and numerous iterations of this technique provide validated toolkits to customize the proteomic discovery platform and maximize the detection and quantification of the labile reversible cysteine O-PTM.[4,11] For example, work by Jennifer van Eyk's laboratory has advanced methodologies to specifically detect S-nitrosylation and measure individual protein thiol-reactivity, thereby discriminating artifacts and ambiguity surrounding site assignment of oxidation.[12,13] Meanwhile, spline-based computational analysis enables extraction of temporal patterns.[14,15] Here, we present the first proteome-wide study of major cysteine modification types in cardiac hypertrophy including reversible O-PTM, $CysSO_2H$, and $CysSO_3H$. We devised a biotin switch-based cysteine O-

Special Issue: Human Proteome Project 2018

Received: May 26, 2018
Published: August 24, 2018

DOI: 10.1021/acs.jproteome.8b00372
J. Proteome Res. XXXX, XXX, XXX−XXX

PTM discovery platform specific for multitime-point quantitative proteomic analysis at different disease stages of hypertrophic progression. To limit nonbiologically oxidized peptides, we selected a maleimide-based reagent for enrichment labeling and combined dimethyl labeling for quantification. Compared to IAM based labeling, maleimide provides higher specificity and reactivity with free thiols.[16,17] In addition, dimethyl based quantitative labeling is highly efficient and cost-effective in studies with large sample size. We implemented the cubic spline-based computational workflow to capture the cysteine O-PTM clusters with distinct temporal profiles and with high association with hypertrophy phenotypic temporal profile. We define proteins in these clusters as molecular signatures. The novelty lies in this being the first study to link global oxidative proteomic signatures to distinct time points of hypertrophic progression, thus showcasing these temporal fingerprints rather than a singular protein or snapshot at a specific time point.

METHODS AND MATERIALS

Experimental Animal Models

Male C57BL/6J mice, 9−12 weeks of age (Jackson Laboratories), were housed in a 12-h light/12-h dark cycle with controlled temperature, humidity, and access to standard chow and water *ad libitum*. Mice were surgically implanted with a subcutaneous micro-osmotic pump (ALZET) delivering 15 mg/kg/day isoproterenol (ISO) (Sigma) or saline vehicle.[18,19] In this treatment protocol, mice developed a gradual cardiac hypertrophy phenotype characterized by significantly increased ejection fraction and HW/BW.[19,20] Independent groups of three mice from each treatment condition were euthanized for sample collection at 1, 3, 5, 7, 10, and 14 days postimplantation. Four technical replicates were performed for each treatment condition. All animal procedures were performed in accordance with the Guide for the Care and Use of Laboratory Animals by the National Research Council and approved by the Animal Research Committee at UCLA.

Biotin Switch-Based Sample Processing

Protein Extraction. Left ventricles were collected from mouse hearts and placed in 1 mL NP-40 lysis buffer (50 mM Tris−HCl, pH 8, 137 mM NaCl, 10% glycerol, 1% NP-40, 2 mM EDTA) containing 100 mM N-ethylmaleimide (NEM) and Halt Protease Inhibitor Cocktail (100X) (ThermoFisher Scientific). Tissue was homogenized using a glass hand homogenizer and mixed by rotation for 2 h at 4 °C before centrifugation at 13 800*g* for 20 min at 4 °C. The protein concentration of the supernatant was measured using the DC protein assay (Bio-Rad).

Biotin Switch-Based Labeling of Reversible Cysteine O-PTM. Aliquots containing 2 mg protein were prepared, then precipitated by 10% trichloroacetic acid (TCA) and centrifuged at 20 000*g* for 15 min at 4 °C. One wash with ice-cold 5% TCA and two washes with 95% ethanol were performed to get rid of small molecules. Pellets were resuspended and alkylated in 1 mL of urea-containing cysteine modification buffer (CMBU) (0.1 M HEPES-NaOH, pH7.4, 1% SDS, 10 mM diethylenetriaminepentaacetic acid [DTPA], 6 M urea) with 0.1 M NEM. After 30 min rotation at room temperature, the samples were reduced by 0.12 M dithiothreitol (DTT) and rotated for another 60 min. To quantify the total abundance of cysteine sites and to preserve cysteine sulfinylation ($CysSO_2H$) and sulfonylation ($CysSO_3H$), 10% of the lysate was reserved as an unlabeled portion and underwent acetone precipitation followed by digestion. For the remaining 90%, proteins were separated from small molecules by centrifugation with 10% TCA, followed by one wash with 5% TCA and two washes with 95% ethanol. Pellets were suspended in 300 μL of CMBU with 0.1 mM maleimide-biotin (Mal-Biotin) (Sigma-Aldrich). After a 30 min rotation at room temperature, unreacted NEM was quenched with 10 mM DTT for an additional 30 min. Small molecules and proteins were separated by TCA and ethanol washes as described above.[21,22]

Digestion and Dimethyl Labeling. Pellets from both labeled and unlabeled portions were solubilized in 0.1 M triethylammonium bicarbonate buffer (TAEB) with 0.1% Rapigest (Waters) and heated at 60 °C for 45 min. Solubilized proteins were alkylated with 9 mM iodoacetamide (IAM) incubation in the dark at room temperature for 30 min. The alkylated lysate underwent trypsin digestion overnight (16 h) at 37 °C with a 1:100 ratio of trypsin to protein. A final concentration of 0.16% (vol/vol) CH_2O or C^2H_2O (Sigma-Aldrich) and 24 mM sodium cyanoborohydride ($NaBH_3CN$) (Sigma-Aldrich) were added to the designated samples with light or medium labeling, respectively. Reciprocal labeling was performed on two out of four technical replicates to minimize the technical bias from dimethyl labeling. After a 1 h incubation at room temperature, 0.16% (vol/vol) ammonium solution was added and mixed for 15 min to quench the reaction.[23−25]

Mal-Biotin Enrichment. Mal-biotin and dimethyl labeled peptides were diluted in 1.2 mL of PBS with 200 μL of prewashed High-Capacity NeutrAvidin slurry (Thermo Scientific). After overnight incubation, the sample was centrifuged, washed twice with 1 mL of PBS, once with 50 mM ammonium bicarbonate with 20% methanol, and eluted with 50% Pierce acetonitrile (ACN) with 0.4% trifluoroacetic acid (TFA).[26]

C18 Column Cleanup. All samples were subjected to 30 min incubation at 37 °C with 1% TFA and centrifugation (13 000*g* for 15 min) to remove remaining Rapigest. Samples were cleaned with Pierce C18 Spin Columns (Thermo Scientific) to remove any interfering substances prior to liquid chromatography−tandem mass spectrometry (LC−MS/MS) analysis.

LC−MS/MS Analysis

LC−MS/MS was performed on digested peptides as done previously.[18,19] To reduce sample complexity and increase protein coverage, we fractionated peptide samples using high-pH/low−pH two-dimensional reversed-phase chromatography prior to MS/MS. Fifty micrograms of peptides was injected into a Phenomenex C18 column (Jupiter Proteo C12, 4-μm particle, 90-Å pore, 100 mm × 1 mm dimension) using a Finnigan Surveyor LC system (Thermo Scientific) for the first-dimension (high-pH) separation. We established a gradient between solvent A (20 mM ammonium formate, pH 10) and solvent B (20 mM ammonium formate, 90% acetonitrile, pH10) at a 50 μL min^{-1} flow-rate with the following timing and solvent proportions: 0−5% solvent B in solvent A from 0−2 min; 5−35% solvent B in solvent A from 3−32 min; and, finally, 80% solvent B in solvent A from 32−37 min. Six fractions of peptides were collected from 16−40 min, lyophilized, and redissolved in 20 μL of 0.5% formic acid with 2% acetonitrile. Each high-pH fraction was injected (10

DOI: 10.1021/acs.jproteome.8b00372
J. Proteome Res. XXXX, XXX, XXX−XXX

μL) to an EasySpray C18 column (PepMap, 3-μm particle, 100-Å pore; 75 μm × 150 mm dimension; Thermo Scientific) using an autosampler on a single Easy-nLC 1000 nano-UPLC system (Thermo Scientific) for second-dimension (low-pH) reversed-phase chromatography analysis. We established a gradient between solvent A (0.1% formic acid, 2% acetonitrile) and solvent B (0.1% formic acid, 80% acetonitrile) at a flow rate of 300 nL min^{-1} with the following timing and solvent proportions: 0−40% solvent B from 0−110 min; 40−80% B from 110−117 min; and 80% B from 117−120 min. Column pressure was maintained below 150 bar. High-resolution LC−MS/MS was performed on a single LTQ Orbitrap Elite instrument (Thermo Scientific) through a Thermo EasySpray interface. MS signals were acquired in Fourier-Transform/Ion-Trap (FT/IT) mode: each FT MS1 survey scan was analyzed at 400 to 2000 m/z mass range and 60 000 resolving power in profile mode, followed by rapid IT MS2 scans on the top 15 ions with monoisotopic peak selection and 3000 intensity threshold. MS2 precursor isolation width was set to 2 m/z, normalized collision energy was 35, and charge state 1 and unassigned charge state were excluded. MS1 and MS2 target ion accumulation targets were 10^4 and 10^6, respectively. MS1 lock mass (m/z 425.120025) and dynamic exclusion (90 s) were used. Throughout the LC−MS/MS experiment, column temperature was held at a constant 50 °C.

Quantification of Cysteine O-PTM Abundance

The acquired raw mass spectra were processed with MaxQuant software[27] version 1.5.6.0 as described.[23] Peptide identification was performed using the Andromeda search engine,[28] against a reverse-decoyed protein sequence database (UniProt Reference Proteome, reviewed, accessed June 12, 2016). This *Mus musculus* proteome (taxonomy ID: 10090) database contains 33 588 canonical sequences and does not include isoform information. Common contaminants were included in the database search. First and main searches were performed with precursor mass tolerances of 20 and 4.5 ppm. Product ion tolerance was set to 0.5 Da. Specificity for trypsin cleavage was required, allowing up to two missed cleavage sites.[29] Dimethylated peptide labels were identified using the "multiplicity" query, including "DimethLys0" and "DimethN-term0" as light labels as well as "DimethLys4" and "DimethN4" as medium labels with a maximum four modified sites for each identified peptide. Variable modification types for enriched samples include Mal-biotin labeled cysteine (451.1889 Da), NEM-labeled cysteine (125.0477 Da), IAM-labeled cysteine (57.0215 Da), and methionine sulfoxidation (15.9949 Da) were queried with a maximum five modified sites for each identified peptide. Variable modification types for unlabeled whole tissue lysate samples include NEM-labeled cysteine (125.0477 Da), IAM-labeled cysteine (57.0215 Da), methionine sulfoxidation (15.9949 Da), $CysSO_2H$ (31.9898 Da), and $CysSO_3H$ (47.9847 Da) were queried with a maximum five modified sites for each identified peptide. Tryptic, semitryptic, and nontryptic peptides within a 20 ppm parent mass window surrounding the candidate precursor mass were searched. Peptide ions from up to three isotopic peaks with fragment mass tolerance of 600 ppm were allowed. Protein inference required ≤5% peptide spectra matching (PSM), posterior error probability (PEP), and ≤1% global level protein false discovery rate (FDR) (Q-value ≤1%), as well as a minimum of two ratio counts. Peptides with a cysteine count lower than one were excluded, along with reverse and potential contaminant flagged peptides. Modified peptide identifications with an Andromeda search score greater than 40, a delta score greater than 6, and a localization probability >0.8 were allowed.[30] All searches for a given data set were based on one set of Andromeda peak list files (apl-files). Each of the cysteine modifications (i.e., Mal-biotin, NEM, IAM, $CysSO_2H$, and $CysSO_3H$) was generated as a separate output file with identified cysteine sites, their extracted ion chromatogram (XIC) values, and normalized ratios of ISO versus vehicle conditions calculated from the differential dimethyl labeled peptides. To ensure data quality, technical replicates with significant change (p-value <0.05) in overall normalized ratio distribution among all four replicates were excluded. The total abundance of one cysteine site is quantified as the sum of XIC values from both modified and unmodified forms of that particular cysteine. Detailed information on number of spectra for identification and quantification, as well as number of unique peptide identified per experimental group are listed in Supplemental Table S-7. Furthermore, number of unique peptides, percent sequence coverage, heavy over light (H/L) ratio of mean peak area (±percent ratio H/L variability), and per protein are listed in Supplemental Table S-8. The mass spectrometry proteomics data have been deposited to the ProteomeXchange Consortium[31] via the PRIDE[32] partner repository with the data set identifier PXD010336.

Data Analysis

Cubic Spline-Based Temporal Clustering. Mal-biotin labeled cysteine sites or total cysteine sites with abundance values for at least four out of six time points in both ISO and vehicle groups were selected for cubic spline-based temporal clustering. The averaged ratio of abundance in ISO to vehicle across replicates was calculated per site. Missing abundance values for a modification site were imputed using average abundance of remaining time-points. After scaling and centering, cubic splines were fitted to ratios across the time points in the R statistical programming language (v3.4.3). The predicted abundance ratios from cubic spline were used for K-mean clustering (kmean package in R) following identification of the cluster numbers (mclust package in R). All the codes used for the analyses were deposited to the Github public repository (https://github.com/UCLA-BD2K/Cubic-Spline-based-Temporal-Analysis-Workflow).

Additional Statistical Analysis. The significance of abundance change in ISO and vehicle conditions was evaluated by a paired two-sided t test. Pearson correlation was performed to analyze the association between phenotype and abundance of Mal-biotin labeled cysteines.

Functional Annotations. Cellular pathway information was retrieved from Reactome (release v63, 2017_12) (https://reactome.org/).[33] To exclude single entity function and nonspecific/generalized pathway terms (e.g., metabolism), enriched pathways are required to house a minimum of two found entities and a maximum of 200 total entities. Significantly enriched pathways are defined by FDR < 0.05 calculated from Fisher's exact test with FDR multiple test correction. neXtProt (release 2018−02) was implemented to annotate the biological processes and disease association of key proteins identified in the analysis.[34]

DOI: 10.1021/acs.jproteome.8b00372
J. Proteome Res. XXXX, XXX, XXX−XXX

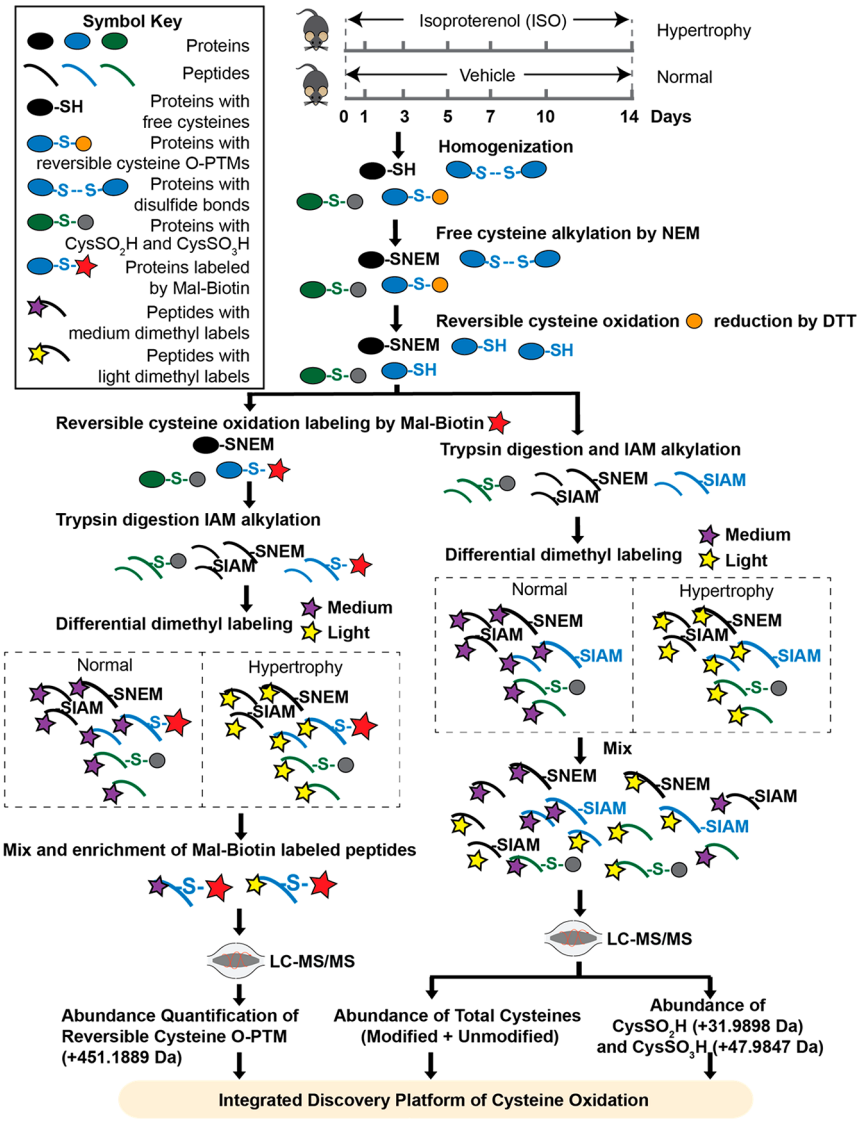

Figure 1. Quantitative cysteine O-PTM proteomics workflow. Left ventricular tissue samples originated from C57BL/6J were subjected to ISO conditions or saline vehicle (vehicle) for 1, 3, 5, 7, 10, and 14 days, with n = 3 mice per group. Extracted proteins underwent biotin switch for reversible cysteine O-PTM labeling. First, free cysteines in the cell lysate were alkylated with NEM to prevent nonspecific labeling of reversible cysteine O-PTM. Subsequently, reversibly oxidized cysteine were reduced with DTT. At this point, 10% of the lysate was separated out for the quantification of the total cysteine sites abundance and DTT-irreversible cysteine O-PTMs (i.e., $CysSO_2H$ and $CysSO_3H$) (right side of flowchart). The remaining 90% (left side of flowchart) was treated with mal-biotin, which labels newly reduced, free cysteine residues. Following trypsin digestion and IAM alkylation of newly exposed free cysteines, lysates from Normal and Hypertrophy groups were differentially labeled with medium/light dimethyl in two of the four technical replicates, whereas the other two received reciprocol labeling. The dimethyl-labeled peptides were quenched by ammonium and equally mixed. The Mal-Biotin labeled portion was enriched by avidin agarose and the abundance of reversible cysteine O-PTM was quantified by LC−MS/MS. Following differential dimethyl labeling, the unlabeled 10% (right side) underwent LC−MS/MS to quantify the abundance of total cysteines and DTT-irreversible cysteine O-PTM. The identification of modified peptide is based on their mass changes by corresponding modifications, that is, + 451.1889 Da for reversible cysteine O-PTM, + 31.9898 Da for $CysSO_2H$, and +47.9847 Da for $CysSO_3H$. Quantification of modifications is based on XIC values. Integrative analysis was performed to characterize the impact of ISO-induced cardiac hypertrophy on the cysteine O-PTM profile. Abbreviations: oxidative post-translational modification (O-PTM); isoproterenol (ISO); N-ethylmaleimide (NEM); dithiothreitol (DTT); cystein sulfinylation ($CysSO_2H$); cystein sulfonylation ($CysSO_3H$); maleimide biotin (Mal-Biotin); extracted ion chromatogram (XIC); iodoacetamide (IAM).

RESULTS AND DISCUSSION

Overview

We developed a cysteine O-PTM discovery platform by integrating a biotin switch-based quantitative proteomics approach with advanced computational analysis, and we applied the novel platform on an ISO-induced cardiac hypertrophic mouse model. First, we defined the abundance distribution of three types of cysteine O-PTM, including reversible O-PTM, $CysSO_2H$, and $CysSO_3H$ during the progression of hypertrophy. Second, we applied statistical analysis to identify key proteins with significantly increased or decreased cysteine O-PTM abundance, followed by cubic spline-based K-mean clustering to dissect the temporal profiles of cysteine O-PTM together with their total cysteine abundance. Third, temporal signatures along with their enriched hypertrophic pathways were identified. Finally, we

DOI: 10.1021/acs.jproteome.8b00372
J. Proteome Res. XXXX, XXX, XXX−XXX

established the association between cysteine O-PTM profiles and hypertrophic phenotypes, keying in on cysteine sites that were significantly correlated with the phenotype dynamics. Integrated analysis of key sites extracted from our computational approaches was performed to comprehensively identify molecular signatures and provide mechanistic insights during the development of cardiac hypertrophy.

Impact of ISO-Induced Hypertrophy on Cysteine O-PTM

Using our cysteine O-PTM discovery pipeline on mouse LV tissue from ISO and vehicle groups (Figure 1), we identified a total of 2505 proteins containing 6818 cysteine sites; with 1655 proteins containing 3324 sites modified by at least one of three cysteine O-PTM types. Specifically, 1095 proteins containing 2162 sites, 484 proteins containing 671 sites, and 447 proteins containing 613 sites were modified by reversible modification, $CysSO_2H$, and $CysSO_3H$, respectively. Among the reversibly modified proteins and cysteine sites, only 167 proteins containing 470 sites and 8 proteins containing 9 sites based on UniProt are known sites of disulfide-bonds and nitrosylated, respectively, revealing that the majority of identified cysteine sites are novel. Figure 2A illustrates the overall change in abundance distribution of reversible cysteine O-PTM over the progression of hypertrophy, with the average abundance of reversible cysteine O-PTM sites across four technical replicates for each time point plotted. All histograms exhibit a J-shaped curve, demonstrating the higher frequency of modified cysteine sites concentrated in the low abundance XIC range. Notably, the distribution of O-PTM abundance in ISO demonstrates a sizable reduction in the lower abundance range, indicating a global enrichment of O-PTM occurring as early as Day3. Figure 2B shows a Venn diagram to depict the number of proteins associated with each individual type of cysteine modification. To summarize, 1057 sites within 377 proteins are unique to an enriched reversible O-PTM proteome, demonstrating the advantage of using enrichment to concentrate less abundant but highly oxidized proteins. The overlapping cysteine sites among three modification types are limited (5 sites), suggesting that the type of cysteine O-PTM is highly site-specific. Comparatively, the numbers of proteins comodified with all three modification types are significantly higher, suggesting that diverse cysteine O-PTM patterns occur on the same protein albeit in a site-specific manner. Overall, these data indicate that the oxidative regulation of proteins requires complex orchestration of myriad oxidative chemistries in a site-specific manner.

We mapped the distribution of O-PTM abundance, expressed as a ratio of ISO over vehicle across six time points in violin plots for the three modification types (Figure 2C). Consistent with 2A, the ratio means of reversible O-PTM on Day 3, 5, 10, and 14 in ISO over vehicle are slightly above zero, demonstrating an increase in reversible O-PTM abundance. $CysSO_2H$ oxidized sites exhibit no distribution change, whereas $CysSO_3H$ oxidized sites have upshifts on Day 5 and 14. The distinct patterns of abundance distribution among the three modification types indicate O-PTM type-specific proteomic regulation during ISO-induced hypertrophy and oxidative stress.

To identify sites of cysteine O-PTM that are significantly altered by ISO treatment, we applied a *t* test on the $\log_2$-transformed fold-change of the reversible cysteine O-PTM (ISO/vehicle) with at least three time points, where a *p*-value < 0.05 and fold-change within the top or bottom 20th

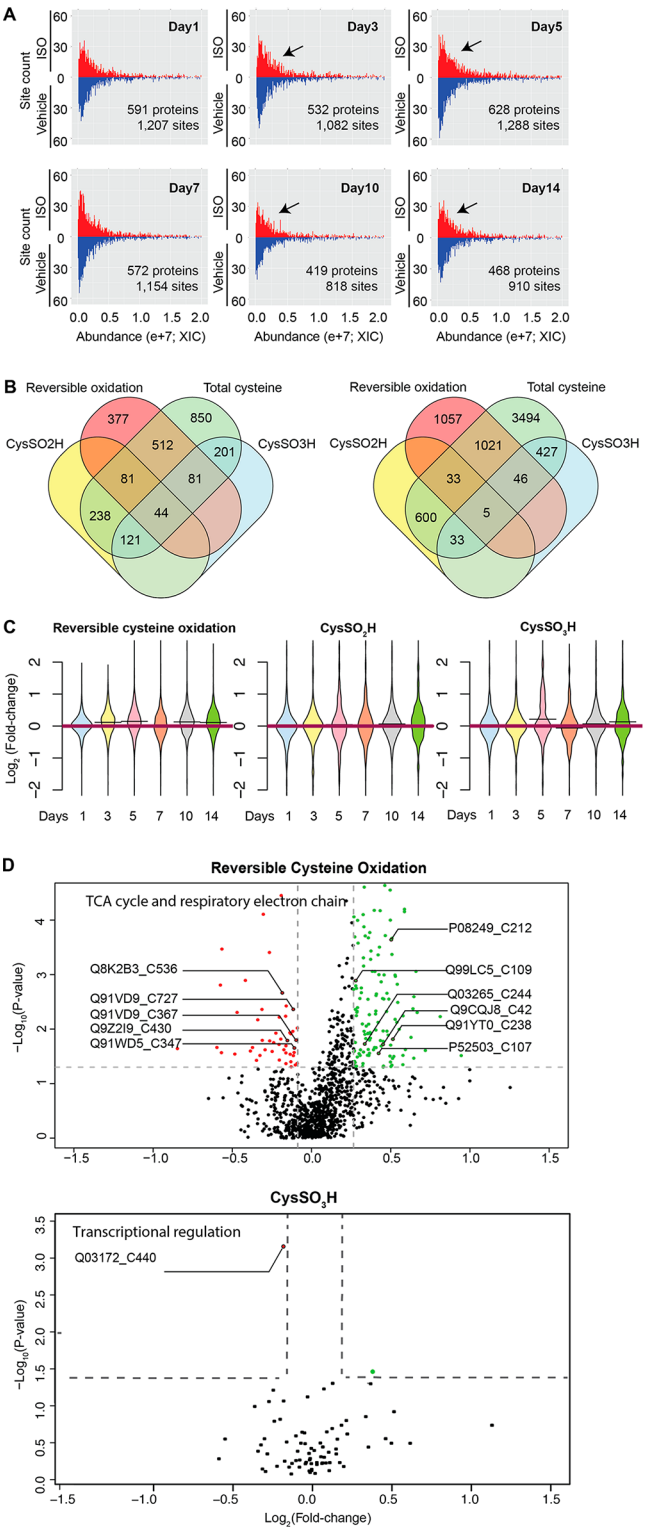

Figure 2. Impact of ISO-induced cardiac hypertrophy on the reversible cysteine O-PTM profile. (A) Abundance distribution of reversible cysteine O-PTM during ISO treatment. Six histograms exhibit the distribution of abundance of reversible cysteine O-PTM in each of the six time-points under both ISO (red) and vehicle (blue) conditions. The absolute value of the vertical axis represents the site counts whereas the horizontal axis represents average abundance value (XIC) across all replicates. The black arrow denotes a significant change in the abundance distribution of ISO occurring on Day 5, where a sizable upshift is observed in the ISO distribution of reversible cysteine O-PTM. (B) Site and protein counts of reversible

DOI: 10.1021/acs.jproteome.8b00372
J. Proteome Res. XXXX, XXX, XXX−XXX

Figure 2. continued

cysteine O-PTM, $CysSO_2H$, and $CysSO_3H$ during ISO-induced hypertrophy. A Venn diagram illustrates the number of reversibly oxidized proteins (left panel) and cysteine sites (right panel) for each of the cysteine O-PTMs that are identified from the integrated discovery platform. Data show that there are considerable and complex patterns of overlap among proteins and sites that are susceptible to modification. (C) Distribution of cysteine O-PTM abundance during ISO treatment. Three violin plots exhibit the log2 transformed abundance ratio of oxidation (y-axis) in ISO versus vehicle over 6 time points across 14 days (x-axis). The red horizontal line depicts the ratio value of zero, demonstrating no change. The black bar on the violin at each time point represents the population mean. The black arrow denotes a significant change in the abundance distribution of ISO occurring on Day5, where a sizable upshift is observed in the ISO distribution of reversible cysteine O-PTM. (D) Statistical validation of changes in oxidative molecular signatures. A volcano plot portrays significantly altered molecular signatures of reversible cysteine O-PTM (top panel) and $CysSO_3H$ (bottom panel) during ISO treatment. Each dot represents a cysteine O-PTM site with respect to its $\log_2$-transformed fold-change of abundance ratio in ISO/vehicle (x-axis) and $-\log_{10}$-transformed p-value from t test (y-axis). Any sites with p-value < 0.05 (horizontal line) and fold-change within the top or bottom 20th percentile (vertical line) are identified as significantly altered molecular signatures. Significantly increased and decreased modification sites are labeled in green and red, respectively. Pathway enrichment by Reactome identified "TCA cycle and respiratory electron chain" as the significantly enriched pathway for signatures with reversible O-PTM. "Transcriptional and translational regulation" is enriched in $CysSO_3H$. The UniProt IDs of proteins housing decreased and increased sites of cysteine O-PTM in these two enriched pathways are labeled. Detailed information regarding proteins of each cluster and their enriched pathways are listed in the Supplemental Tables S-1 and S-2, respectively. Abbreviations: oxidative post-translational modification (O-PTM); isoproterenol (ISO); cystein sulfinylation ($CysSO_2H$); cystein sulfonylation ($CysSO_3H$); extracted ion chromatogram (XIC); TCA cycle and respiratory electron transport (TCA).

percentile were deemed significant. For reversible cysteine O-PTM (Figure 2D, top panel), we found 128 sites within 74 proteins with significantly increased abundance and 46 sites within 39 proteins with significantly decreased abundance during ISO treatment, marking their potential to be signatures of cardiac hypertrophy. In addition, one and two $CysSO_3H$ oxidized sites are significantly increased and decreased, respectively (Figure 2D, lower panel).

Reactome identified 17 and 55 pathways that are enriched by proteins with significantly increased and decreased reversible cysteine sites, respectively (Figure 2D, top panel). Specifically, proteins with significantly decreased reversibly oxidized sites are significantly enriched in three extracellular matrix organization and signaling pathways, two ion homeostasis and transportation pathways, and two TCA cycle and respiratory electron transport (TCA) pathway. Proteins with significantly increased reversibly oxidized cysteine sites are significantly enriched in seven transcriptional and translational regulation, two post-translational modification (PTM) of protein, two glucose metabolism, and three TCA cycle and respiratory electron transport pathways. Notably, the "TCA cycle and respiratory electron transport" pathway is enriched in both significantly increased and decreased sites with associated proteins are labeled by their UniProt ID. This observation reveals a significant and diverse reversible O-PTM regulation on mitochondrial metabolism during ISO-induced cardiac hypertrophy. In addition, significantly increased cysteine modification on protein susceptible to methylation and phosphorylation indicates further hierarchical interactions between PTMs. Zinc finger factor, ZEP1 is significantly decreased in $CysSO_3H$ (associated proteins are labeled by their UniProt ID), demonstrating redox regulation of transcriptional regulation during hypertrophy. Detailed information on featured sites, proteins, and their enriched pathways are listed in Supplemental Tables S-1 and S-2, respectively.

Integrated Temporal Profiles of Cysteine O-PTM in Hypertrophic Heart Proteome

To characterize the dynamic patterns of reversible cysteine O-PTM during the progression of cardiac hypertrophy, we calculated the abundance ratios of each reversible cysteine O-PTM site in ISO over vehicle for 1, 3, 5, 7, 10, and 14 days and employed a cubic spline-based smoothing approach for data denoising. The cubic spline-fitted data were subsequently classified by K-means clustering to produce a total of eight unique dynamic patterns (Figure 3A). The largest cluster (Cluster 6, n = 198) remains unchanged during ISO treatment. These likely represent structural disulfide cysteines of housekeeping proteins. Consistent with this notion, reactome analysis identified extracellular matrix (ECM) organization and signaling pathways to be enriched in this cluster, and ECM proteins are known to be rich in structural disulfide bonds.

The dynamic patterns of eight clusters were represented in the stripcharts with smoothing lines, demonstrating the temporal feature of each cluster (Figure 3B). Different temporal patterns of reversible O-PTM clusters may reveal the hidden association between dynamic regulation of biological processes and the progression of cardiac hypertrophy. We applied determination coefficient analysis to extract key sites as temporal signatures that are highly correlated (R^2 > 0.8) with the temporal feature of their corresponding clusters. Cluster 6, with its lack of significant temporal changes to cysteine sites, is excluded from temporal signatures analysis. Among a total of 415 sites within 250 proteins that match the criteria as temporal signatures, the majority (404 sites within 243 proteins) are modified by reversible cysteine O-PTM, whereas five sites within four proteins by $CysSO_2H$ and six sites within five proteins by $CysSO_3H$. Notably, majority of $CysSO_2H$ sites (3 out of 5) are distributed in Cluster 1, exhibiting a continual decrease whereas the majority of $CysSO_3H$ sites (5 out of 6) are enriched in Cluster 7, exhibiting a continual increase. Notably, $CysSO_2H$ can be enzymatically reduced to free cysteine and can also be further oxidized into $CysSO_3H$, which is nonreducible.[35,36] These observations revealed distinct regulation pattern of different irreversible modification types during ISO-induced oxidative stress. Specifically, $CysSO_2H$ on Cys164 and $CysSO_3H$ on Cys167 in ATP7b (Q64446) shared the temporal pattern of continual increase (Cluster 7), suggesting an inactivation of ATP7b during cardiac hypertrophy. As a malfunction in ATP7b leads to cellular copper accumulation and cardiomyopathy in Wilson disease,[37] the mapping of ATP7b's irreversible O-PTM temporal pattern offers mechanistic insights into cardiac complications of Wilson disease.

In a total of 243 reversibly oxidized proteins, 62 out of 90 bore at least two sites that fall into more than one temporal cluster. The distinct temporal regulation of cysteine sites within the same protein is possibly due to the unique microenvironment of the particular cysteine sites (e.g., cysteine

DOI: 10.1021/acs.jproteome.8b00372
J. Proteome Res. XXXX, XXX, XXX−XXX

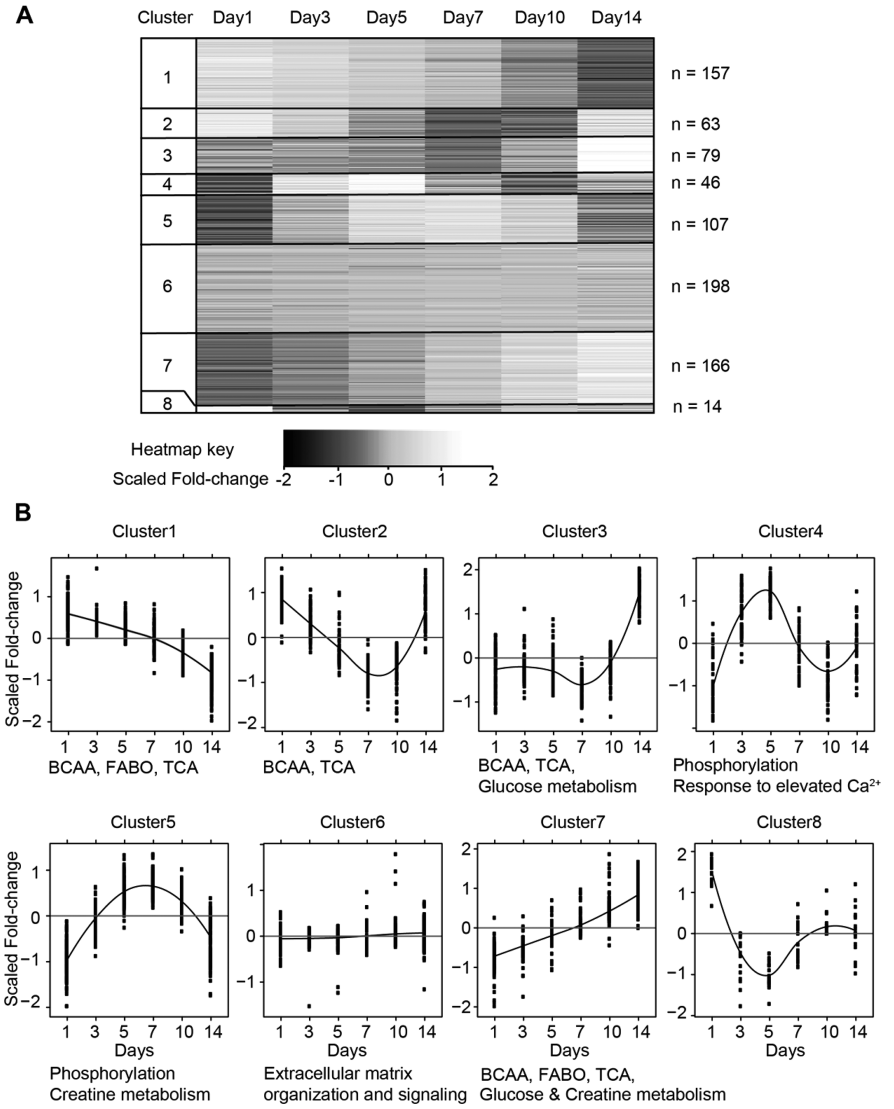

Figure 3. Temporal profiling of reversible cysteine O-PTM proteomes using cubic spline-based clustering. (A) Temporal mapping of the reversible cysteine O-PTM proteome. Cubic spline followed by K-mean clustering was applied to abundance ratio of reversible cysteine O-PTM sites in ISO versus vehicle across 6 time points (*x*-axis), as represented by a scale from two-fold decrease (black) to two-fold increase (white), in a heat map. Our analyses yielded eight unique temporal patterns of change in the reversible cysteine O-PTM abundance ratio. The numbers of sites of each cluster are as listed to the right the heatmap. (B) Cluster-specific temporal patterns of reversible cysteine O-PTM. Eight stripcharts exhibit the trends in the normalized abundance ratio of reversible cysteine O-PTM sites (ISO vs vehicle; *Y*-axis) over six time points (*x*-axis). Cluster 1 of reversible cysteine O-PTM sites is characterized by continual decrease; Cluster 2 by an initial decrease that dips on Day 7; Cluster 3 by a sharp increase after Day 7; Cluster 4 by a sinusoidal curve with an initial increase that shifts to decrease on Day 5 and back to increase on Day 10; Cluster 5 by an arched curve that peaks on Day 7; Cluster 6 by no change; Cluster 7 by continual increase; and Cluster 8 by an initial sharp decrease that dips on Day 5. Key cysteine sites and pathways are listed on the stripcharts of their corresponding clusters. Detailed information regarding proteins of each cluster and their enriched pathways are listed in the Supplemental Tables S-3 and S-4, respectively. Abbreviations: oxidative post-translational modification (O-PTM); isoproterenol (ISO); TCA cycle and respiratory electron transport (TCA); branched-chain amino acid (BCAA) catabolism; fatty acid beta-oxidation (FABO).

pK_a, enzymatic interaction). We utilized Reactome to perform pathway enrichment with temporal signature proteins that are unique to one cluster. Cluster 1 is characterized by a continual decrease and significantly enriched in branched-chain amino acid (BCAA) catabolism, fatty acid beta-oxidation (FABO), and TCA pathways; Cluster 2 by an initial decrease that dips on Day 7 and significantly enriched in BCAA and TCA pathways; Cluster 3 by a sharply increase after Day 7 and significantly enriched in BCAA, TCA, and glucose metabolism; Cluster 4 by a sinusoidal curve and significantly enriched in protein phosphorylation and complement cascade; Cluster 5 by an arched curve that peaks on Day 7 and significantly enriched in protein phosphorylation and creatine metabolism; Cluster 6 by no change and significantly enriched in extracellular matrix organization and signaling; and Cluster 7 by a continual increase and significantly enriched in BCAA, FABO, TCA, glucose metabolism, and creatine metabolism; and Cluster 8 by an initial sharp decrease before returning to baseline levels. Reversible cysteine O-PTM sites/proteins with significant alteration in abundance ratio across 14 days after ISO were widely distributed among eight clusters, suggesting that dynamic temporal patterns is a state-of-the-art measurement and prediction that is independent of the absolute value of end-point measurements. Specifically, three 40S ribosomal

DOI: 10.1021/acs.jproteome.8b00372
J. Proteome Res. XXXX, XXX, XXX−XXX

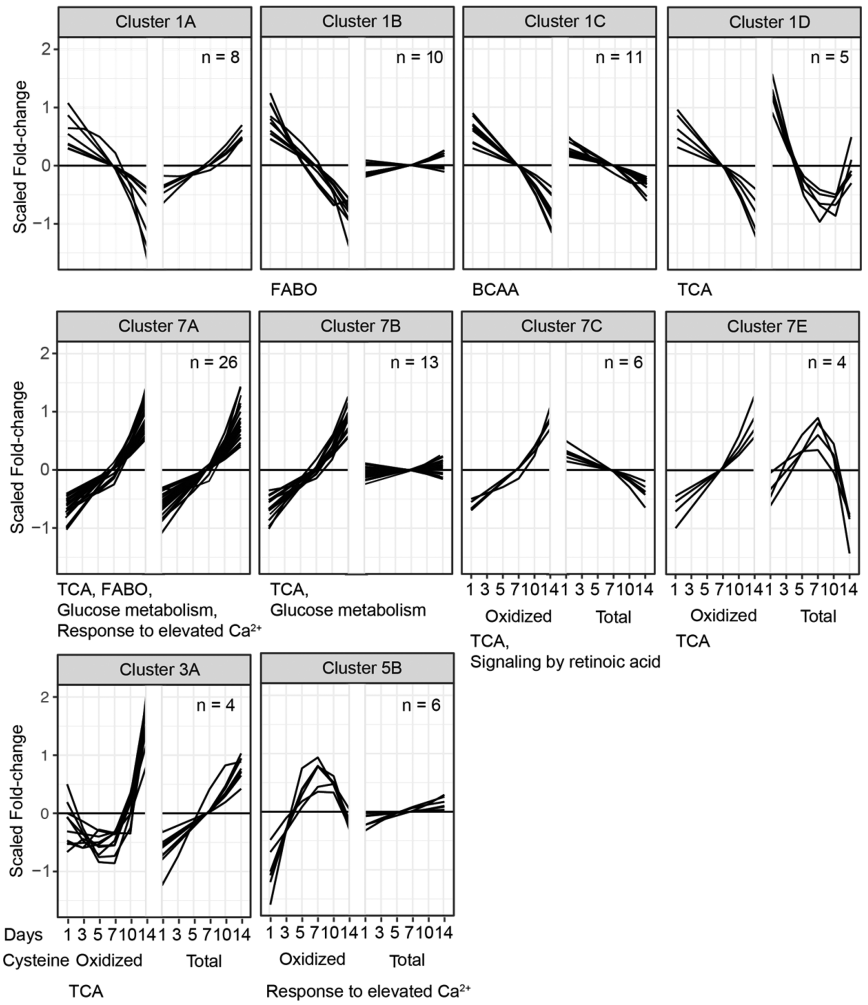

Figure 4. Temporal profiling combining reversible cysteine O-PTM and total cysteine proteomes using cubic spline-based coclustering. Cubic spline followed by K-mean clustering was applied to abundance ratio of total cysteine sites (ISO vs vehicle) in the proteome. The profiles of reversible cysteine O-PTM temporal signatures (Figure 3: $R^2 > 0.8$) were coplotted with the well-fitted temporal profiles of their total cysteine abundance (labeled as A−E; $R^2 > 0.8$). Ten coclusters with more than three cysteine sites were identified and demonstrated in the stripcharts, exhibiting the trends in the normalized abundance ratio of reversible cysteine O-PTM and total cysteine sites (y-axis) over six time points (x-axis). As previously described, Cluster 1 of reversible cysteine O-PTM sites is characterized by continual decrease; Cluster 3 by a sharp increase after Day7; Cluster 5 by an arched curve that peaks on Day 7; Cluster 6 by no change; and Cluster 7 by continual increase. Cluster A of total cysteine sites is characterized by continual increase; Cluster B by no change; Cluster C by continual decrease; Cluster D by initial sharp decrease that dips between Day 7−10; Cluster E by an arched curve that peaks on Day 7. Key pathways are listed on the stripcharts of their corresponding clusters. Detailed information regarding proteins of each cluster and their enriched pathways is listed in the Supplemental Tables S-3 and S-4, respectively. Abbreviations: oxidative post-translational modification (O-PTM); isoproterenol (ISO); TCA cycle and respiratory electron transport (TCA); branched-chain amino acid (BCAA) catabolism; fatty acid beta-oxidation (FABO).

proteins, S3, S6, and S11, with significantly increased oxidation abundance are enriched in Cluster 1 (continual decrease), suggesting an initial wave of sharply increased oxidation in response to ISO treatment that diminishes as the heart hypertrophies. Notably, the majority of glucose metabolism proteins (4 out of 5) with significantly increased abundance belong to Cluster 7, demonstrating a strong and significant increase of reversible cysteine O-PTM in glucose metabolism during cardiac hypertrophy. In addition, the conserved Cys17 in the ATPase domain of the cytosolic chaperone protein, Hspa8, was continually oxidized (Cluster 7). As the perpetual oxidation of the conserved cysteine in the ER chaperone, Hspa5, has been shown to enhance chaperone function and ER homeostasis, the perpetual oxidation of Hspa8 indicates a potential function in cytosolic protein homeostasis during ISO-induced cardiac hypertrophy.[21,22,38]

The stoichiometry is an important feature of PTM and can be calculated by comparing the abundance of a modified form with all forms of a site of interest. Integrating the temporal patterns of total cysteine abundance and reversible cysteine O-PTM further reveals the comprehensive regulation of cysteine O-PTM stoichiometry. We applied cubic spline based clustering on total cysteine abundance and subsequently coclustered temporal patterns of reversible cysteine O-PTM with total cysteine abundance (Figure 4). Briefly, cubic spline-based K-mean clustering was implemented to determine the temporal clusters of the total cysteine proteome. Subsequently, temporal signature sites of total cysteines from each cluster were extracted by determination coefficient analysis with $R^2 > 0.8$ as described and combined with the temporal pattern of oxidized cysteine sites. Clusters with more than three sites

DOI: 10.1021/acs.jproteome.8b00372
J. Proteome Res. XXXX, XXX, XXX−XXX

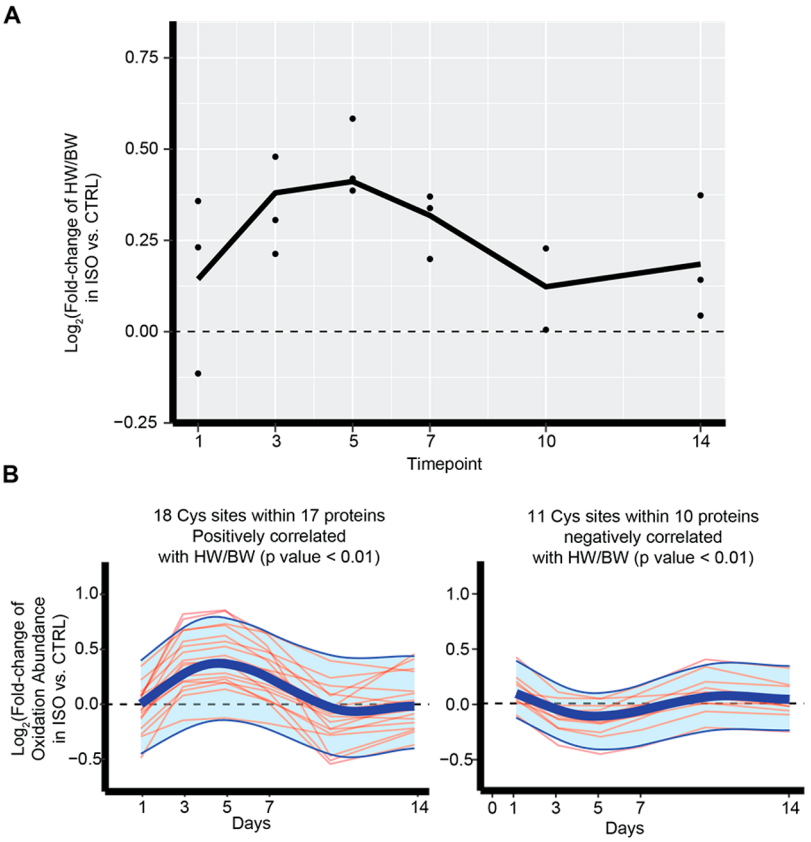

Figure 5. Phenotypic alteration and corresponding cysteine site fingerprints during ISO-induced cardiac hypertrophy. (A) HW/BWs were temporally measured three times per time point during ISO-induced cardiac remodeling (time points Day 1, 3, 5, 7, 10, and 14) and subsequently normalized to HW/BWs of vehicle. The majority of log2 transformed measurements showed positive values, indicating HW/BWs of ISO mice increase relative to that of vehicle mice, as expected. The difference of HW/BWs between ISO and vehicle mice was continuously broadened and peaked at Day 5, and then decreased until Day 10, stabilizing thereafter. (B) Twenty-nine cysteine sites, which are highly correlated with HW/BW changes, were identified through Pearson correlation coefficient (p-value <0.01); their abundance ratios were displayed over time. The left panel shows 18 cysteine sites within 17 proteins positively correlated with HW/BW, while the right panel shows 11 cysteine sites within ten proteins that are negatively correlated with HWBW. The red line indicates each cysteine site and the thick blue line shows the average trend of the group. The two thin blue lines indicate upper bound and lower bound that cover 95% of the data. Detailed information regarding proteins of each cluster and their enriched pathways are listed in the Supplemental Tables S-5 and S-6, respectively. Abbreviations: isoproterenol (ISO); heart weight-body weight ratio (HW/BW); control (CTRL).

were considered as conserved patterns and included in the subsequent analysis.

Figure 4 shows a total of 10 coclusters with more than three sites were identified. These coclusters consist of three temporal patterns from reversible and irreversible cysteine modification identified previously and four newly identified temporal patterns from total cysteine abundance. Cluster 1A is characterized by continual decrease in oxidation with continual increase in total abundance, suggesting a decrease in oxidation occupancy, Cluster 1B by continual decreased oxidation with no change in total abundance and enriched in fatty acid metabolism, Cluster 1C by continual decrease in both oxidation and total abundance and enriched in branched chain amino acid catabolism, Cluster 1D by continual decreased oxidation with initial decreased abundance that dips on Day 7 and enriched in respiratory electron transport, Cluster 7A by both continual increase in oxidation and total abundance and enriched in glucose metabolism, FABO, and lipoprotein remodeling, Cluster 7B by continual increased oxidation with no change in total abundance and enriched in glucose metabolism and ATP synthesis, Cluster 7C by continual increased oxidation with decreased total abundance and enriched in retinoic acid signaling, suggesting a continual increase in cysteine O-PTM occupancy in regulating retinoic acid, which contributes to cardiac development, Cluster 7E by continual increase oxidation with arched curve that peaks on Day 7, Cluster 3A by initial decreased oxidation that dips on Day 7 with continual increased total abundance and enriched in pyruvate metabolism and TCA cycle, and Cluster 5B by an arched curve that peaks on Day 7 with no change in total abundance. In addition to sites modified by reversible O-PTM, two $CysSO_3H$ sites bore the temporal pattern of Cluster 7A. Notably, three major enriched pathways from Cluster1, BCAA, FABO, and TCA, were divided into Cluster 1B, 1C, and 1D, according to the temporal patterns of their total cysteine abundance, demonstrating the clustering of their temporal pattern is dependent on their biological function. Among clusters with altered stoichiometry during cardiac hypertrophy, Cluster 1B and Cluster 7B are enriched in FABO and glucose metabolism, respectively. As cardiac hypertrophy is featured by an increased reliance on glucose with an overall reduced fatty acid metabolism,[39] these observations provide a detailed molecular map that reveals an additional layer of regulation in mitochondrial energy metabolism via reversible cysteine O-PTM. Detailed information on featured sites, proteins, and

DOI: 10.1021/acs.jproteome.8b00372
J. Proteome Res. XXXX, XXX, XXX−XXX

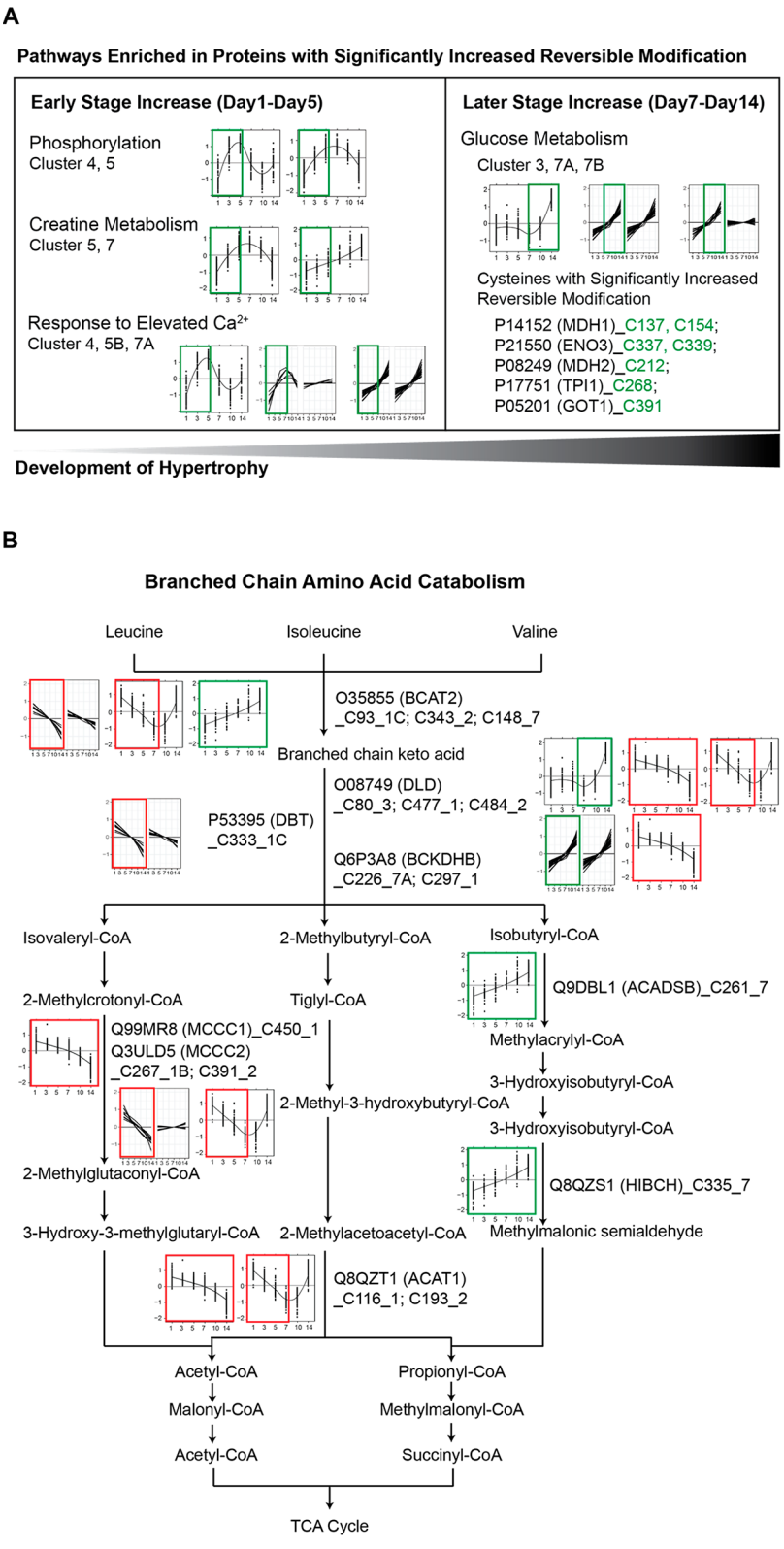

Figure 6. Signature pathways and proteins contribute to cardiac hypertrophy. (A) Temporal changes of modified cysteine sites on pathways enriched in proteins with significantly increased modification abundance. Pathways and the temporal changes of their corresponding enriched temporal clusters are illustrated. Temporal cluster with increased trend of modification change at indicated duration are boxed and color-coded as green. Protein phosphorylation, creatine metabolism, and response to elevated Ca^{2+} pathways are increased at early stage of hypertrophy whereas glucose metabolism has a trend of increased modification at later stage of hypertrophy. Cysteine sites with significantly increased modification in glucose metabolism pathway are labeled with accession number, protein name, and modified cysteine site. These cysteine sites with significantly increased modification are color-coded as green. (B) Temporal changes of modified cysteine sites on BCAA pathway proteins are labeled and illustrated. Each molecular player is labeled with accession number, protein name, modified cysteine site, and temporal cluster. Temporal cluster with increased or decreased trend at indicated duration are boxed and color-coded as green or red, respectively. Most sites in the shared pathways

DOI: 10.1021/acs.jproteome.8b00372
J. Proteome Res. XXXX, XXX, XXX−XXX

Figure 6. continued

among BCAA pathways exhibit diverse temporal trend. Notably, valine catabolism pathway exhibits an increased trend of cysteine modification whereas the temporal trend of leucine and isoleucine is decreased at early stage of hypertrophy. These observations suggest that oxidative cysteine regulation of BCAA pathway is highly compartmentalized by biological function. Abbreviations: branched-chain amino acid catabolism (BCAA).

their enriched pathways by temporal profiling analysis is listed in Supplemental Tables S-3 and S-4, respectively.

Correlation between Hypertrophy Phenotype and Cysteine O-PTM Abundance

Temporal cluster analysis revealed the intrinsic temporal regulation of a cysteine O-PTM site, which may contribute to or respond to the dynamic pattern of the cardiac hypertrophy phenotype. The heart weight−body weight (HW/BW) ratios of the mouse strain were documented along with the left ventricle sample collections to provide temporal phenotypic profiles. During ISO treatment, all mouse strains exhibited cardiac hypertrophy development starting from Day 1 post ISO-treatment (Figure 5A). The averaged ratio of HW/BW across six time points increased 20% in ISO over vehicle. Interestingly, we observed an arched curve of hypertrophy development that peaked on Day 5 (33% higher than control) and stabilized on Day 10 (∼14% higher than control). This is consistent with previous observations of the ISO mouse model in C57BL/6J.[40]

To directly map the association between temporal change of cysteine O-PTM and that of the hypertrophy phenotype, we performed cubic spline-based Pearson correlation. We selected 29 cysteine O-PTM sites with a p-value < 0.01 as key oxidation sites that significantly associated with cardiac hypertrophy. Among them, 18 cysteine sites within 17 proteins and 11 cysteine sites within 10 proteins were positively and negatively correlated with HW/BW changes, respectively (Figure 5B). Pathway enrichment of proteins with a positive correlation to phenotype unveiled four secretory proteins in the extracellular space that regulate Insulin-like Growth Factor (IGF) transport, a key regulatory mechanism of cardiac hypertrophy.[41,42] In addition, a BCAA pathway protein, MCCC2, was identified in both correlation groups, demonstrating a diverse regulation of MCCC2 cysteine O-PTM. Notably, reversible O-PTM of an additional two key BCAA proteins, BCAT2 and DBT, were observed in Cluster 1C, featured by continually decreased oxidation and total cysteine abundance. As a BCAA catabolic defect is a metabolic hallmark of the failing heart,[43] diverse oxidative regulation of BCAA proteins can potentially contribute to hypertrophy by metabolic reprogramming. Detailed information on featured sites, proteins, and their enriched pathways are listed in Supplemental Tables S-5 and S-6, respectively.

Signature Pathways and Proteins That Contribute to Cardiac Hypertrophy

Combining molecular signatures from differential analysis, cubic spline-based temporal clustering, and phenotypic correlation, we highlighted seven biological processes that are reproducibly identified as signature pathways during cardiac hypertrophy, including TCA, FABO, BCAA, glucose metabolism, protein phosphorylation, creatine metabolism, and response to elevated Ca^{2+}. Specifically, among pathways enriched in proteins with significantly increased reversible modification, protein phosphorylation, creatine metabolism, and response to elevated Ca^{2+} pathways exhibited an increase in cysteine modification in early stages of hypertrophy, whereas glucose metabolism pathways were modified in the later stages (Figure 6A). Comparatively, the cysteine oxidative profiles of TCA, FABO, and BCAA were more complicated, as metabolic reprogramming is a highly integrative process with complex compensatory mechanisms. We mapped all identified BCAA pathway proteins and their corresponding temporal dynamics. As expected, temporal trends of cysteine modification differ across pathways and even among cysteine sites within one protein. Interestingly, cysteine temporal profiles of valine catabolism subpathways exhibit a trend toward increase, whereas that of leucine and isoleucine catabolism uniformly illustrates a decreased trend at early stage of hypertrophy. These observations demonstrate that cysteine O-PTM profiles are highly correlated with key biological processes during cardiac hypertrophy. Furthermore, these integrated molecular signatures of hypertrophy are novel and can be used to define phenotypes of metabolic reprogramming in new and informative ways.

Role of Cysteine O-PTM in Cardiovascular Biology

ISO induced beta-adrenoceptor stimulation has been shown to evoke cardiac oxidative stress.[44,45] Specifically, this process is mediated through increased mitochondrial ROS production, as mitochondrial targeted antioxidant diminish oxidative stress and its downstream biological events.[46] Meanwhile, the capacity of nitric oxide synthesis is also increased in response ISO, likely from enhanced expression of endothelial and inducible nitric oxide synthases.[47] During heart failure development, elevated RO/NS production in turn leads to modification of reactive cysteine thiol groups. The highly reactive thiol group of cysteine residues has made it difficult to isolate native versus nonbiological oxidized peptides in the cardiovascular system, and subsequently, to elucidate their biological role. Pioneering studies on both technological and biological fronts have overcome this barrier and broken new ground in cardiovascular medicine. Recent work from Jennifer van Eyk's laboratory identified distinct subpopulations of nitrosylated cysteines through a dual-labeling of nitrosylation that reduces labeling bias.[26] This advanced methodology was then utilized to explore glycogen synthase kinase 3β (GSK3β) regulation by nitrosylation and it was discovered that nitrosylation reduces GSK3β kinase activity and promotes its nuclear translocation.[48]

The biological and physiological roles of cysteine O-PTM in both vascular systems and cardiac muscle have been pioneered and carried into clinical translation by the work of Jonathan Stamler and Elizabeth Murphy, respectively. A seminal paper in 2004 by the Stamler laboratory was the first demonstration of a role of nitrosylation in innate immunity and vascular function.[49] Mice devoid of S-nitrosoglutathione reductase showed marked increased in nitrosylation, vascular damage, and mortality following endotoxic challenge. More recent work unveiled a role for the hemoglobin β Cys93 residue in nitrosylation-based vasoactivity, demonstrating that S-nitrosohemoglobin plays a role in cardioprotection.[50] This and other notable contributions[51−53] have revolutionized our understanding of cysteine O-PTM in vascular signaling.

DOI: 10.1021/acs.jproteome.8b00372
J. Proteome Res. XXXX, XXX, XXX−XXX

Studies from Elizabeth Murphy's lab have advanced knowledge of cysteine O-PTM in cardiac muscle biology. This group pioneered novel labeling approaches for measuring nitrosylation occupancy, the fraction of a given protein that is nitrosylation modified in the myocardium, and demonstrated that nitrosylation occupancy levels following ischemic preconditioning protect against cysteine O-PTM.[54] More recent, formative work by this lab demonstrated increased nitrosylation abundance at Cys144 of the cardioprotective protein, TRIM72, is a molecular switch preventing TRIM72 degradation following an oxidative insult, which increases cardiomyocyte survival.[55] Other work unveiled complex profiles of nitroso-redox signaling and nitrosylation of cardiac proteins in failing versus nonfailing human cardiac tissue. Sex-specific differences in S-glutathionylation of endothelial nitric oxide synthase were discovered, adding to the overall complexity of these pathways in cardiac muscle.[56]

Our measurements represent the sum of all types of cysteine O-PTM events including disulfide bonds, nitrosylation, glutathionylation, and irreversible cysteine O-PTMs. Among these modifications, different modifications result from diverse regulatory mechanisms[4] and modifications can be interconvertible. For example, glutathionylation of Cys63 on the ER stress protein BiP is mediated by sulfenylation.[21] Meanwhile, both sulfenylation and glutathionylation of BiP have been shown to enhance BiP's activity in preventing aggregation. Meanwhile, different modifications can also lead to distinct biological consequences. For example, two types of oxidative posttranslational modifications have been shown to occur on Cys674 of SERCA2: reversible S-glutathiolation increases SERCA activity, whereas irreversible oxidative $CysSO_3H$ is associated with decreased activity.[57] Conventionally, irreversible modifications were considered to be markers of cellular damage. Yet recently advances suggest that these modifications have regulatory capacities. For example, the unique active cysteine sites of nitrile hydratase and thiocyanate hydrolase are responsible for metal coordination and can be modified by $CysSO_2H$. The fully reduced forms of these two enzymes appear inactive, suggesting that $CysSO_2H$ is critical in maintaining their catalytic activity.[58,59] Our study provides key signatures modified by reversible and irreversible cysteine O-PTMs, facilitating the target prioritization for studying hierarchical regulation among different types of cysteine O-PTMs.

Technical Considerations and Future Directions

Capitalizing on several modified variations of biotin switch method,[23,60] we developed a quantitative approach for in-depth characterization of the cysteine oxidized cardiac proteome. First, NEM alkylates free cysteines via a faster, more specific Michael addition reaction than the nucleophilic substitution reaction with IAM.[16,17] Efficient labeling with less pH dependence makes NEM a great choice to preserve the labile reversible cysteine O-PTM and minimize artificial chemical alteration and nonspecific labeling during sample processing over IAM. Second, biotin maleimide labeling offers the efficiency and specificity accompanying the Michael addition reaction. In addition, as the avidin−biotin interaction is strong and rapid,[61] enrichment with high-capacity NeutrAvidin agarose enables a large-scale pull-down with high efficiency. Third, stable-isotope dimethyl labeling using reductive amination is a reliable widely used approach in MS-based quantitative proteomics.[25,62] Specifically, dimethylation enhances fragmentation efficiency of collision-induced dissociation (CID) by increasing the number of positive charges on a peptide.[63] In addition, high cost-effectiveness makes dimethylation applicable for studies with any sample size.

Nevertheless, there are a few limitations to consider. The multistage process, including biotin maleimide labeling, dimethyl labeling, and avidin enrichment requires milligrams of starting material. The development of biotin maleimide-based isotope reagents would be a great tool to combine this two-stage labeling. While DTT is a potent and efficient reducing reagent for all types of reversible cysteine O-PTM, proteins with a large number of stable disulfide bonds will be prevalently enriched in this assay. On the other hand, this method can facilitate discovery of functional and catalytic disulfide bonds and less reactive cysteine O-PTMs that require more potent reductant. Despite the limitations mentioned above, our biotin switch-based reversible cysteine discovery platform provides a reliable workflow allowing robust detection of reversible cysteine sites at multiple time points during cardiac hypertrophy development.

To comprehensively understand the impact of ISO-induced hypertrophy on cysteine O-PTM sites and proteins identified from this robust biotin switch based quantitative proteomic approach, we used a bioinformatics approach that dissects the temporal pattern of the cysteine O-PTM proteome using a cubic spline-based K-mean clustering.[15,64] The cubic spline method generates a fitted curve for all the cysteine O-PTM abundance values across time points for each oxidation site. This denoising method extracts the most fitted temporal pattern from a group of highly variable values with cross-validation. The smoothed temporal curve facilitates the subsequent unsupervised clustering to accurately identify temporal clusters of interests. However, the assumption of this method is that alteration across time points is gradual and smooth; this will potentially have a trade-off with a sudden alteration between time points that is biologically significant. Thus, more time points are required or multiple temporal analysis methods widely used in the genomics field, including advanced pattern extraction,[65] can be adapted and applied to reveal the true biological signal from the technical bias.

CONCLUSIONS

Utilizing a novel cysteine O-PTM discovery platform composed of customized redox proteomics and advanced computational analysis, we present the first proteome-wide study of multitype cysteine O-PTM on the well-known mouse model of ISO-induced cardiac hypertrophy. The novelty and strength of our study lie in our ability to cluster the temporal behavioral profiles of cysteine residues and visualize distinct patterns of change as well as how they correlate to the hypertrophic phenotype. The advanced computational and statistical platform enabled us to create a dynamic and integrated picture of the entire cysteine oxidative proteome, a molecular signature that can be used for in-depth profiling and defining of various health and diseased states.

ASSOCIATED CONTENT

Supporting Information

The Supporting Information is available free of charge on the ACS Publications website at DOI: 10.1021/acs.jproteome.8b00372.

DOI: 10.1021/acs.jproteome.8b00372
J. Proteome Res. XXXX, XXX, XXX−XXX

List of cysteine sites with alterations in modification abundance during cardiac hypertrophy; enriched biological pathways of proteins bearing cysteine sites with significantly increased/decreased modification abundance; grouped cysteine sites identified from cubic spline-based temporal clustering; enriched biological pathways of proteins associated with cysteine sites identified from cubic spline-based temporal clustering; list of cysteine sites significantly correlated with hypertrophy phenotype; enriched biological pathways of proteins associated with cysteine sites that are significantly correlated with hypertrophy phenotype; summary information on raw file contents and statistics for all experimental groups (PDF)

Summary information and statistics of identified proteins in each experimental group (XLSX)

AUTHOR INFORMATION

Corresponding Author

*E-mail: ppingucla@gmail.com. Phone: 310-267-5624.

ORCID

Peipei Ping: 0000-0002-4974-9587

Author Contributions

¶J.W. and H.C. contributed equally to this work. J.W. contributed to study design, data acquisition, data analysis, data management, and manuscript writing. H.C. contributed to data analysis, data management, and manuscript writing. These authors contributed equally to this work. N.C.C. contributed to data analysis. Q.C. contributed to animal experimental model and data acquisition. D.C.M.N. contributed to the data acquisition. B.M. contributed to data analysis. S.B.S. contributed to manuscript writing. D.W. contributed to manuscript writing. A.O.G. contributed to critical revisions of the manuscript and data management. P.P. contributed to study design, funding acquisition, and manuscript writing.

Notes

The authors declare no competing financial interest.

The mass spectrometry proteomics data have been deposited to the ProteomeXchange Consortium via the PRIDE partner repository with the data set identifier PXD010336.

ACKNOWLEDGMENTS

This study was supported in part by US National Institutes of Health funding R35-HL135772 and U54-GM114833 to P.P.

REFERENCES

(1) Shimizu, I.; Minamino, T. Physiological and pathological cardiac hypertrophy. *J. Mol. Cell. Cardiol.* **2016**, *97*, 245−62.

(2) Maulik, S. K.; Kumar, S. Oxidative stress and cardiac hypertrophy: a review. *Toxicol. Mech. Methods* **2012**, *22* (5), 359−66.

(3) Souders, C. A.; Borg, T. K.; Banerjee, I.; Baudino, T. A. Pressure overload induces early morphological changes in the heart. *Am. J. Pathol.* **2012**, *181* (4), 1226−35.

(4) Murray, C. I.; Van Eyk, J. E. Chasing cysteine oxidative modifications: proteomic tools for characterizing cysteine redox status. *Circ.: Cardiovasc. Genet.* **2012**, *5* (5), 591.

(5) Lim, A.; Prokaeva, T.; McComb, M. E.; Connors, L. H.; Skinner, M.; Costello, C. E. Identification of S-sulfonation and S-thiolation of a novel transthyretin Phe33Cys variant from a patient diagnosed with familial transthyretin amyloidosis. *Protein Sci.* **2003**, *12* (8), 1775−85.

(6) Pastore, A.; Piemonte, F. Protein glutathionylation in cardiovascular diseases. *Int. J. Mol. Sci.* **2013**, *14* (10), 20845−76.

(7) Sag, C. M.; Santos, C. X.; Shah, A. M. Redox regulation of cardiac hypertrophy. *J. Mol. Cell. Cardiol.* **2014**, *73*, 103−11.

(8) Alcock, L. J.; Perkins, M. V.; Chalker, J. M. Chemical methods for mapping cysteine oxidation. *Chem. Soc. Rev.* **2018**, *47* (1), 231−268.

(9) Forrester, M. T.; Stamler, J. S. A classification scheme for redox-based modifications of proteins. *Am. J. Respir. Cell Mol. Biol.* **2007**, *36* (2), 135−7.

(10) Bechtel, T. J.; Weerapana, E. From structure to redox: The diverse functional roles of disulfides and implications in disease. *Proteomics* **2017**, *17* (6), 1600391.

(11) Jaffrey, S. R.; Snyder, S. H. The biotin switch method for the detection of S-nitrosylated proteins. *Sci. Signaling* **2001**, *2001* (86), pl1.

(12) Murray, C. I.; Chung, H. S.; Uhrigshardt, H.; Van Eyk, J. E. Quantification of mitochondrial S-nitrosylation by CysTMT(6) switch assay. *Methods Mol. Biol.* **2013**, *1005*, 169−79.

(13) Murray, C. I.; Uhrigshardt, H.; O'Meally, R. N.; Cole, R. N.; Van Eyk, J. E. Identification and quantification of S-nitrosylation by cysteine reactive tandem mass tag switch assay. *Mol. Cell. Proteomics* **2012**, *11* (2), M111.013441.

(14) Liu, T. Y.; Huang, H. H.; Wheeler, D.; Xu, Y.; Wells, J. A.; Song, Y. S.; Wiita, A. P. Time-Resolved Proteomics Extends Ribosome Profiling-Based Measurements of Protein Synthesis Dynamics. *Cell systems* **2017**, *4* (6), 636−644.

(15) Bhasi, K.; Forrest, A.; Ramanathan, M. SPLINDID: a semi-parametric, model-based method for obtaining transcription rates and gene regulation parameters from genomic and proteomic expression profiles. *Bioinformatics* **2005**, *21* (20), 3873−9.

(16) Kramer, P. A.; Duan, J.; Qian, W. J.; Marcinek, D. J. The Measurement of Reversible Redox Dependent Post-translational Modifications and Their Regulation of Mitochondrial and Skeletal Muscle Function. *Front. Physiol.* **2015**, *6*, 347.

(17) Reisz, J. A.; Bechtold, E.; King, S. B.; Poole, L. B.; Furdui, C. M. Thiol-blocking electrophiles interfere with labeling and detection of protein sulfenic acids. *FEBS J.* **2013**, *280* (23), 6150−61.

(18) Lau, E.; Cao, Q.; Lam, M. P. Y.; Wang, J.; Ng, D. C. M.; Bleakley, B. J.; Lee, J. M.; Liem, D. A.; Wang, D.; Hermjakob, H.; Ping, P. Integrated omics dissection of proteome dynamics during cardiac remodeling. *Nat. Commun.* **2018**, *9* (1), 120.

(19) Lau, E.; Cao, Q.; Ng, D. C.; Bleakley, B. J.; Dincer, T. U.; Bot, B. M.; Wang, D.; Liem, D. A.; Lam, M. P.; Ge, J.; Ping, P. A large dataset of protein dynamics in the mammalian heart proteome. *Sci. Data* **2016**, *3*, 160015.

(20) Drews, O.; Tsukamoto, O.; Liem, D.; Streicher, J.; Wang, Y.; Ping, P. Differential regulation of proteasome function in isoproterenol-induced cardiac hypertrophy. *Circ. Res.* **2010**, *107* (9), 1094−101.

(21) Wang, J.; Sevier, C. S. Formation and Reversibility of BiP Protein Cysteine Oxidation Facilitate Cell Survival during and post Oxidative Stress. *J. Biol. Chem.* **2016**, *291* (14), 7541−57.

(22) Wang, J.; Pareja, K. A.; Kaiser, C. A.; Sevier, C. S. Redox signaling via the molecular chaperone BiP protects cells against endoplasmic reticulum-derived oxidative stress. *eLife* **2014**, *3*, e03496.

(23) Garcia-Santamarina, S.; Boronat, S.; Domenech, A.; Ayte, J.; Molina, H.; Hidalgo, E. Monitoring in vivo reversible cysteine oxidation in proteins using ICAT and mass spectrometry. *Nat. Protoc.* **2014**, *9* (5), 1131−45.

(24) Gu, L.; Robinson, R. A. A simple isotopic labeling method to study cysteine oxidation in Alzheimer's disease: oxidized cysteine-selective dimethylation (OxcysDML). *Anal. Bioanal. Chem.* **2016**, *408* (11), 2993−3004.

(25) Boersema, P. J.; Raijmakers, R.; Lemeer, S.; Mohammed, S.; Heck, A. J. Multiplex peptide stable isotope dimethyl labeling for quantitative proteomics. *Nat. Protoc.* **2009**, *4* (4), 484−94.

(26) Chung, H. S.; Murray, C. I.; Venkatraman, V.; Crowgey, E. L.; Rainer, P. P.; Cole, R. N.; Bomgarden, R. D.; Rogers, J. C.; Balkan, W.; Hare, J. M.; Kass, D. A.; Van Eyk, J. E. Dual Labeling Biotin Switch Assay to Reduce Bias Derived From Different Cysteine

DOI: 10.1021/acs.jproteome.8b00372
J. Proteome Res. XXXX, XXX, XXX−XXX

Subpopulations: A Method to Maximize S-Nitrosylation Detection. *Circ. Res.* **2015**, *117* (10), 846−57.
(27) Cox, J.; Mann, M. MaxQuant enables high peptide identification rates, individualized p.p.b.-range mass accuracies and proteome-wide protein quantification. *Nat. Biotechnol.* **2008**, *26* (12), 1367−72.
(28) Cox, J.; Neuhauser, N.; Michalski, A.; Scheltema, R. A.; Olsen, J. V.; Mann, M. Andromeda: a peptide search engine integrated into the MaxQuant environment. *J. Proteome Res.* **2011**, *10* (4), 1794−805.
(29) van der Reest, J.; Lilla, S.; Zheng, L.; Zanivan, S.; Gottlieb, E. Proteome-wide analysis of cysteine oxidation reveals metabolic sensitivity to redox stress. *Nat. Commun.* **2018**, *9* (1), 1581.
(30) Bogdanow, B.; Zauber, H.; Selbach, M. Systematic Errors in Peptide and Protein Identification and Quantification by Modified Peptides. *Mol. Cell. Proteomics* **2016**, *15* (8), 2791−801.
(31) Deutsch, E. W.; Csordas, A.; Sun, Z.; Jarnuczak, A.; Perez-Riverol, Y.; Ternent, T.; Campbell, D. S.; Bernal-Llinares, M.; Okuda, S.; Kawano, S.; Moritz, R. L.; Carver, J. J.; Wang, M.; Ishihama, Y.; Bandeira, N.; Hermjakob, H.; Vizcaino, J. A. The ProteomeXchange consortium in 2017: supporting the cultural change in proteomics public data deposition. *Nucleic Acids Res.* **2017**, *45* (D1), D1100−D1106.
(32) Vizcaino, J. A.; Csordas, A.; Del-Toro, N.; Dianes, J. A.; Griss, J.; Lavidas, I.; Mayer, G.; Perez-Riverol, Y.; Reisinger, F.; Ternent, T.; Xu, Q. W.; Wang, R.; Hermjakob, H. 2016 update of the PRIDE database and its related tools. *Nucleic Acids Res.* **2016**, *44* (22), 11033.
(33) Fabregat, A.; Jupe, S.; Matthews, L.; Sidiropoulos, K.; Gillespie, M.; Garapati, P.; Haw, R.; Jassal, B.; Korninger, F.; May, B.; Milacic, M.; Roca, C. D.; Rothfels, K.; Sevilla, C.; Shamovsky, V.; Shorser, S.; Varusai, T.; Viteri, G.; Weiser, J.; Wu, G.; Stein, L.; Hermjakob, H.; D'Eustachio, P. The Reactome Pathway Knowledgebase. *Nucleic Acids Res.* **2018**, *46* (D1), D649−D655.
(34) Gaudet, P.; Michel, P. A.; Zahn-Zabal, M.; Britan, A.; Cusin, I.; Domagalski, M.; Duek, P. D.; Gateau, A.; Gleizes, A.; Hinard, V.; Rech de Laval, V.; Lin, J.; Nikitin, F.; Schaeffer, M.; Teixeira, D.; Lane, L.; Bairoch, A. The neXtProt knowledgebase on human proteins: 2017 update. *Nucleic Acids Res.* **2017**, *45* (D1), D177−D182.
(35) Lowther, W. T.; Haynes, A. C. Reduction of cysteine sulfinic acid in eukaryotic, typical 2-Cys peroxiredoxins by sulfiredoxin. *Antioxid. Redox Signaling* **2011**, *15* (1), 99−109.
(36) Woo, H. A.; Jeong, W.; Chang, T. S.; Park, K. J.; Park, S. J.; Yang, J. S.; Rhee, S. G. Reduction of cysteine sulfinic acid by sulfiredoxin is specific to 2-cys peroxiredoxins. *J. Biol. Chem.* **2005**, *280* (5), 3125−8.
(37) Patil, M.; Sheth, K. A.; Krishnamurthy, A. C.; Devarbhavi, H. A review and current perspective on Wilson disease. *J. Clin. Exp. Hepatol.* **2013**, *3* (4), 321−36.
(38) O'Donnell, J. P.; Marsh, H. M.; Sondermann, H.; Sevier, C. S. Disrupted Hydrogen-Bond Network and Impaired ATPase Activity in an Hsc70 Cysteine Mutant. *Biochemistry* **2018**, *57* (7), 1073−1086.
(39) Kolwicz, S. C., Jr.; Tian, R. Glucose metabolism and cardiac hypertrophy. *Cardiovasc. Res.* **2011**, *90* (2), 194−201.
(40) Rau, C. D.; Wang, J.; Avetisyan, R.; Romay, M. C.; Martin, L.; Ren, S.; Wang, Y.; Lusis, A. J. Mapping genetic contributions to cardiac pathology induced by Beta-adrenergic stimulation in mice. *Circ.: Cardiovasc. Genet.* **2015**, *8* (1), 40−9.
(41) Hua, Y.; Zhang, Y.; Ren, J. IGF-1 deficiency resists cardiac hypertrophy and myocardial contractile dysfunction: role of microRNA-1 and microRNA-133a. *Journal of cellular and molecular medicine* **2012**, *16* (1), 83−95.
(42) Troncoso, R.; Ibarra, C.; Vicencio, J. M.; Jaimovich, E.; Lavandero, S. New insights into IGF-1 signaling in the heart. *Trends Endocrinol. Metab.* **2014**, *25* (3), 128−37.
(43) Sun, H.; Olson, K. C.; Gao, C.; Prosdocimo, D. A.; Zhou, M.; Wang, Z.; Jeyaraj, D.; Youn, J. Y.; Ren, S.; Liu, Y.; Rau, C. D.; Shah, S.; Ilkayeva, O.; Gui, W. J.; William, N. S.; Wynn, R. M.; Newgard, C. B.; Cai, H.; Xiao, X.; Chuang, D. T.; Schulze, P. C.; Lynch, C.; Jain, M. K.; Wang, Y. Catabolic Defect of Branched-Chain Amino Acids Promotes Heart Failure. *Circulation* **2016**, *133* (21), 2038−49.
(44) Zhang, G. X.; Kimura, S.; Nishiyama, A.; Shokoji, T.; Rahman, M.; Yao, L.; Nagai, Y.; Fujisawa, Y.; Miyatake, A.; Abe, Y. Cardiac oxidative stress in acute and chronic isoproterenol-infused rats. *Cardiovasc. Res.* **2005**, *65* (1), 230−8.
(45) Zhang, G. X.; Ohmori, K.; Nagai, Y.; Fujisawa, Y.; Nishiyama, A.; Abe, Y.; Kimura, S. Role of AT1 receptor in isoproterenol-induced cardiac hypertrophy and oxidative stress in mice. *J. Mol. Cell. Cardiol.* **2007**, *42* (4), 804−11.
(46) Andersson, D. C.; Fauconnier, J.; Yamada, T.; Lacampagne, A.; Zhang, S. J.; Katz, A.; Westerblad, H. Mitochondrial production of reactive oxygen species contributes to the beta-adrenergic stimulation of mouse cardiomycytes. *J. Physiol.* **2011**, *589* (7), 1791−801.
(47) Krenek, P.; Kmecova, J.; Kucerova, D.; Bajuszova, Z.; Musil, P.; Gazova, A.; Ochodnicky, P.; Klimas, J.; Kyselovic, J. Isoproterenol-induced heart failure in the rat is associated with nitric oxide-dependent functional alterations of cardiac function. *Eur. J. Heart Failure* **2009**, *11* (2), 140−6.
(48) Wang, S. B.; Venkatraman, V.; Crowgey, E. L.; Liu, T.; Fu, Z.; Holewinski, R.; Ranek, M.; Kass, D. A.; O'Rourke, B.; Van Eyk, J. E. Protein S-Nitrosylation Controls Glycogen Synthase Kinase 3beta Function Independent of Its Phosphorylation State. *Circ. Res.* **2018**, *122* (11), 1517−1531.
(49) Liu, L.; Yan, Y.; Zeng, M.; Zhang, J.; Hanes, M. A.; Ahearn, G.; McMahon, T. J.; Dickfeld, T.; Marshall, H. E.; Que, L. G.; Stamler, J. S. Essential roles of S-nitrosothiols in vascular homeostasis and endotoxic shock. *Cell* **2004**, *116* (4), 617−28.
(50) Zhang, R.; Hess, D. T.; Reynolds, J. D.; Stamler, J. S. Hemoglobin S-nitrosylation plays an essential role in cardioprotection. *J. Clin. Invest.* **2016**, *126* (12), 4654−4658.
(51) Stomberski, C. T.; Hess, D. T.; Stamler, J. S. Protein S-Nitrosylation: Determinants of Specificity and Enzymatic Regulation of S-Nitrosothiol-Based Signaling. *Antioxid. Redox Signaling* **2012**, *00*, 000−000.
(52) Seth, D.; Stamler, J. S. SNOs Differ: Methodological and Biological Implications. *Circ. Res.* **2015**, *117* (10), 826−9.
(53) Gonzalez, D. R.; Treuer, A.; Sun, Q. A.; Stamler, J. S.; Hare, J. M. S-Nitrosylation of cardiac ion channels. *J. Cardiovasc. Pharmacol.* **2009**, *54* (3), 188−95.
(54) Kohr, M. J.; Aponte, A.; Sun, J.; Gucek, M.; Steenbergen, C.; Murphy, E. Measurement of S-nitrosylation occupancy in the myocardium with cysteine-reactive tandem mass tags: short communication. *Circ. Res.* **2012**, *111* (10), 1308−12.
(55) Kohr, M. J.; Evangelista, A. M.; Ferlito, M.; Steenbergen, C.; Murphy, E. S-nitrosylation of TRIM72 at cysteine 144 is critical for protection against oxidation-induced protein degradation and cell death. *J. Mol. Cell. Cardiol.* **2014**, *69*, 67−74.
(56) Menazza, S.; Aponte, A.; Sun, J.; Gucek, M.; Steenbergen, C.; Murphy, E. Molecular Signature of Nitroso-Redox Balance in Idiopathic Dilated Cardiomyopathies. *J. Am. Heart Assoc.* **2015**, *4* (9), e002251.
(57) Qin, F.; Siwik, D. A.; Lancel, S.; Zhang, J.; Kuster, G. M.; Luptak, I.; Wang, L.; Tong, X.; Kang, Y. J.; Cohen, R. A.; Colucci, W. S. Hydrogen peroxide-mediated SERCA cysteine 674 oxidation contributes to impaired cardiac myocyte relaxation in senescent mouse heart. *J. Am. Heart Assoc.* **2013**, *2* (4), e000184.
(58) Murakami, T.; Nojiri, M.; Nakayama, H.; Odaka, M.; Yohda, M.; Dohmae, N.; Takio, K.; Nagamune, T.; Endo, I. Post-translational modification is essential for catalytic activity of nitrile hydratase. *Protein Sci.* **2000**, *9* (5), 1024−30.
(59) Arakawa, T.; Kawano, Y.; Katayama, Y.; Nakayama, H.; Dohmae, N.; Yohda, M.; Odaka, M. Structural basis for catalytic activation of thiocyanate hydrolase involving metal-ligated cysteine modification. *J. Am. Chem. Soc.* **2009**, *131* (41), 14838−43.
(60) Li, R.; Huang, J.; Kast, J. Identification of total reversible cysteine oxidation in an atherosclerosis model using a modified biotin switch assay. *J. Proteome Res.* **2015**, *14* (5), 2026−35.

DOI: 10.1021/acs.jproteome.8b00372
J. Proteome Res. XXXX, XXX, XXX−XXX

(61) Haugland, R. P.; You, W. W. Coupling of antibodies with biotin. *Methods in molecular biology* **2008**, *418*, 13−24.
(62) Hsu, J. L.; Huang, S. Y.; Chow, N. H.; Chen, S. H. Stable-isotope dimethyl labeling for quantitative proteomics. *Anal. Chem.* **2003**, *75* (24), 6843−52.
(63) Fu, Q.; Li, L. De novo sequencing of neuropeptides using reductive isotopic methylation and investigation of ESI QTOF MS/MS fragmentation pattern of neuropeptides with N-terminal dimethylation. *Anal. Chem.* **2005**, *77* (23), 7783−95.
(64) Straube, J.; Gorse, A. D.; Team, P. C. o. E.; Huang, B. E.; Le Cao, K. A. A Linear Mixed Model Spline Framework for Analysing Time Course 'Omics' Data. *PLoS One* **2015**, *10* (8), e0134540.
(65) Tchagang, A. B.; Bui, K. V.; McGinnis, T.; Benos, P. V. Extracting biologically significant patterns from short time series gene expression data. *BMC Bioinf.* **2009**, *10*, 255.

DOI: 10.1021/acs.jproteome.8b00372
J. Proteome Res. XXXX, XXX, XXX−XXX